

**Gas pulsation-assisted fluidization of cohesive micron powder
An X-ray imaging study**

Wu, Kaiqiao; Kamphorst, Rens; van der Sande, P. Christian; Wagner, Evert C.; Meesters, Gabrie M.H.; van Ommen, J. Ruud

DOI

[10.1016/j.ces.2025.121529](https://doi.org/10.1016/j.ces.2025.121529)

Publication date

2025

Document Version

Final published version

Published in

Chemical Engineering Science

Citation (APA)

Wu, K., Kamphorst, R., van der Sande, P. C., Wagner, E. C., Meesters, G. M. H., & van Ommen, J. R. (2025). Gas pulsation-assisted fluidization of cohesive micron powder: An X-ray imaging study. *Chemical Engineering Science*, 310, Article 121529. <https://doi.org/10.1016/j.ces.2025.121529>

Important note

To cite this publication, please use the final published version (if applicable).
Please check the document version above.

Copyright

Other than for strictly personal use, it is not permitted to download, forward or distribute the text or part of it, without the consent of the author(s) and/or copyright holder(s), unless the work is under an open content license such as Creative Commons.

Takedown policy

Please contact us and provide details if you believe this document breaches copyrights.
We will remove access to the work immediately and investigate your claim.



Gas pulsation-assisted fluidization of cohesive micron powder: An X-ray imaging study

Kaiqiao Wu ^{a,b,*}, Rens Kamphorst ^b, P. Christian van der Sande ^b, Evert C. Wagner ^b,
Gabrie M.H. Meesters ^b, J. Ruud van Ommen ^{b,*}

^a School of Chemical Engineering and Light Industry, Guangdong University of Technology, Guangzhou, 510006, China

^b Faculty of Applied Sciences, Delft University of Technology, Delft, 2629HZ, the Netherlands

ARTICLE INFO

Keywords:

Pulsed flow
Process intensification
Cohesive powder
Assistance method
Gas channel

ABSTRACT

Conventional fluidization of cohesive powders is challenging due to their strong interparticle forces, often requiring assistance methods. In this study, the hydrodynamics of pulsed and vibrated beds of cohesive Geldart C silica powder (Sauter mean diameter $d_{32} = 7.9 \mu\text{m}$) in a 19.2 cm diameter column were investigated using X-ray imaging. The results show that low-frequency, moderate-amplitude gas pulsation improves fluidization by disrupting long, persistent gas channels. Higher-frequency pulsation is dampened throughout the bed, resulting in negligible improvement over unassisted systems. When coupled with mechanical vibration, gas pulsation slightly mitigates solid compaction at the bottom section, but the overall flow pattern remains largely unchanged compared to vibration alone. The findings highlight the potential of integrating gas pulsation with other assistance methods to enhance fluidization in practical applications.

1. Introduction

Over the last decades, the fluidization of granular materials has been extensively studied and has found applications in various industries, including chemical, waste conversion, pharmaceutical, biotechnological, and functional materials (Grace, 2020), due to its excellent gas-solids interaction. However, when dealing with particles smaller than around $30 \mu\text{m}$, fluidization becomes challenging as these particles exhibit cohesiveness due to dominant interparticle forces (Kamphorst et al., 2023). The fluidization of such powders often results in channeling, slugging, and excessive agglomeration, leading to poor gas-solid contact and, consequently, an ineffective fluidization process. Various methods have been proposed to address these limitations. Examples include mechanical vibration (Mawatari et al., 2015; Kamphorst et al., 2024a; Wu et al., 2023a), mechanical agitation (Alavi and Caussat, 2005; Wu et al., 2024; van der Sande et al., 2025), acoustic vibration (Chirone et al., 2018; Ammendola and Chirone, 2010), micro-jets (van Ommen et al., 2013; Nasri Lari et al., 2020) and pulsed flows (Ireland et al., 2016).

Amongst these assistance methods, gas pulsation is categorized as a non-intrusive method, and excels in its flexibility and compatibility, as it can be directly implemented by adding butterfly or solenoid valves to existing flow supply setups. With these advantages, gas pulsation has attracted interest in the community as a means to improve the fluidization

behavior (Saidi et al., 2019). Identified as a method of process intensification, previous studies have demonstrated that pulsed flow operation can effectively alter the fluidization of Geldart A and B types of particles, leading to improved powder mixing (Akhavan et al., 2008), enhanced drying (Jia et al., 2016; Liu et al., 2017), and tight control over flow patterns (Wu et al., 2017, 2025).

Despite these advancements, few attempts have been conducted to investigate the use of gas pulsation to improve the fluidization of cohesive Geldart C group powders. Akhavan et al. (2015) demonstrated that square-wave pulsed flows are able to effectively eliminate gas channels and initiate the fluidization of various types of nano-silica, which significantly reduces the minimum fluidization velocity, U_{mf} , by up to 72%. Additionally, they observed that U_{mf} decreases with increasing pulsation frequency within the range of 1.5 to 5.0 Hz. Ali and Asif (2012) studied the effects of square waves at different frequencies on the fluidization of hydrophilic fumed nanosilica. They noted that varying the frequency of the pulsed flow within a narrow range of 0.05 to 0.25 Hz led to a substantial reduction in both agglomerate size and U_{mf} . Building on this work, Al-Ghurabi et al. (2020) employed square-wave pulsations at a frequency of 0.05 Hz, and found a minor reduction in U_{mf} compared to unassisted fluidization, attributing this effect to the breakup of large agglomerates. They also assessed the agglomerate diameter based on the analysis of the bed pressure drop, and found

* Corresponding authors.

E-mail addresses: Kaiqiao.Wu@gdut.edu.cn (K. Wu), J.R.vanOmmen@tudelft.nl (J. Ruud van Ommen).

<https://doi.org/10.1016/j.ces.2025.121529>

Received 12 January 2025; Received in revised form 28 February 2025; Accepted 12 March 2025

Available online 15 March 2025

0009-2509/© 2025 The Author(s). Published by Elsevier Ltd. This is an open access article under the CC BY license (<http://creativecommons.org/licenses/by/4.0/>).

Nomenclature

D	inner diameter of the column (cm)
Ct	time-averaged frame at flow time t (-)
S	similarity between two consecutive frames (-)
t_c	stable channel time (s)
ε	time-averaged normalized gas fraction (-)
ε_r	normalized gas fraction (-)
I_{full}	X-ray intensity of full reference (-)
I_{empty}	X-ray intensity of empty reference (-)
I_0	X-ray intensity from the source (-)
d	material thickness (m)
μ	attenuation coefficient (1/m)
I	X-ray intensity on the detector (-)
Y	position in vertical direction (cm)
H	bed height (cm)
H_0	initial bed height (cm)
ΔP	measured pressure drop (mbar)
ΔP_0	static pressure drop (mbar)
U_{mf}	minimum fluidization velocity (cm/s)
$N_{\Delta t}$	number of frames over a chosen time interval (-)
t	time (s)
A	pulse amplitude (cm/s)
M	mean gas velocity (cm/s)
A_v	vibration amplitude (mm)
f_v	vibration frequency (Hz)
f	pulsation frequency (Hz)
U_0	superficial gas velocity (cm/s)
d_{32}	Sauter mean diameter (μm)

that gas pulsation reduced the agglomerate size by more than 14 % compared to unassisted fluidization. However, studies focusing on cohesive micropowders ($1 \mu\text{m} \leq d_{32} \leq 30 \mu\text{m}$) are notably scarce, leaving this field largely unexplored. Ali et al. (2021), through the measurement of fractional pressure drop, reported that a pulsed fluidized bed of hydrophilic fumed nanosilica could lead to the segregation of agglomerates along the bed height, rather than creating homogeneous fluidization. Khosravi Bizhaem and Basirat Tabrizi (2013) concluded that the effect of gas pulsation on the fluidization of cohesive micropowders is less pronounced than on larger particles. Using square waves, they found that increasing the frequency (in the range of 1 to 10 Hz) results in a transition from channeling to bubbling-like fluidization of $10 \mu\text{m}$ alumina powder.

Due to the opaqueness of the column, studies of bed hydrodynamics were primarily limited to direct visualization of the flow patterns near the wall region. As a result, the bubbles within the column were not clearly distinguishable, making it challenging to assess the fluidization behavior of the gas-solids mixture. Non-intrusive technique X-ray imaging has been widely applied to study gas-solid fluidization across various powders and geometries. By capturing the attenuation of X-ray beams through the gas-solid suspension, X-ray imaging provides time-resolved flow patterns, allowing for the monitoring of key hydrodynamic events, including bubble motion (Ma et al., 2019a), gas channel breakage (Gómez-Hernández et al., 2017), bubble eruption (Macri et al., 2020), particle circulation (Iannello et al., 2022), and transitions between different flow regimes (Saayman et al., 2013), within a larger three-dimensional (3D) cylindrical column.

In this study, the impact of pulsed flow on promoting the fluidization of cohesive micro-silica powder is investigated, as part of our series exploring various assistance methods, following recent studies of vibration (Wu et al., 2023a) and stirring methods (Wu et al., 2024). The present study considers the effects of various parameters on flow patterns, including pulsation frequency, amplitude and their combined effects with mechanical vibration. A fast X-ray imaging technique was

employed to examine bed hydrodynamics. An in-depth analysis of flow patterns and gas channel properties, extracted from the X-ray images, along with measurements of bed pressure drop, was conducted to assess fluidization quality and behavior. Additionally, the combined effects of pulsed flow and mechanical vibration were explored.

2. Methods and materials

2.1. Experimental setup

Fig. 1 depicts a schematic representation of the experimental arrangement. The experiments were conducted in a Plexiglas cylindrical column with an inner diameter, D , of 19.2 cm. A 3 mm thick SIKA-R 3AX porous plate (grade efficiency: $1.9 \mu\text{m}$, bubble pressure point: 54 mbar) was used to couple the column to a plenum chamber positioned below, ensuring an even gas distribution throughout the cross-sectional area of the column. To mitigate powder loss during experimentation, a breakout box was positioned atop the column. Additionally, a wash bottle and a High Efficiency Particulate Air (HEPA) powder filter were installed prior to the discharge point of the fluidizing gas, ensuring a healthy and safe work environment.

To thoroughly evaluate the quality of fluidization, pressure drop and pressure fluctuations were measured. Differential pressure transducers (OMEGA-PX419 and UNIK-5000) were affixed to the lateral wall, probing the gas pressure at the distributor plate surface, the breakout box, and 27.5 cm above the distributor plate ($H/D = 1.43$). Pressure oscillations were recorded at a rate of 1000 Hz.

To attain an initial bed height-to-diameter ratio (H_0/D) of approximately 1.7, 1406 g of silica micro-powder was loaded into the column. The particles were fluidized under ambient conditions with dry nitrogen gas to eliminate the possible effects of capillary forces. Data acquisition was conducted using an in-house LabVIEW program interfaced with the flow controller, flow meters, and pressure transducers. The column was mounted on a vibration table, which was utilized in designated experiments to provide vertical vibration. When applied, the vertical vibration was maintained at an amplitude, A_v , of 1 mm and a frequency, f_v , of 30 Hz, which were previously found to be most effective for the same powder (Wu et al., 2023a).

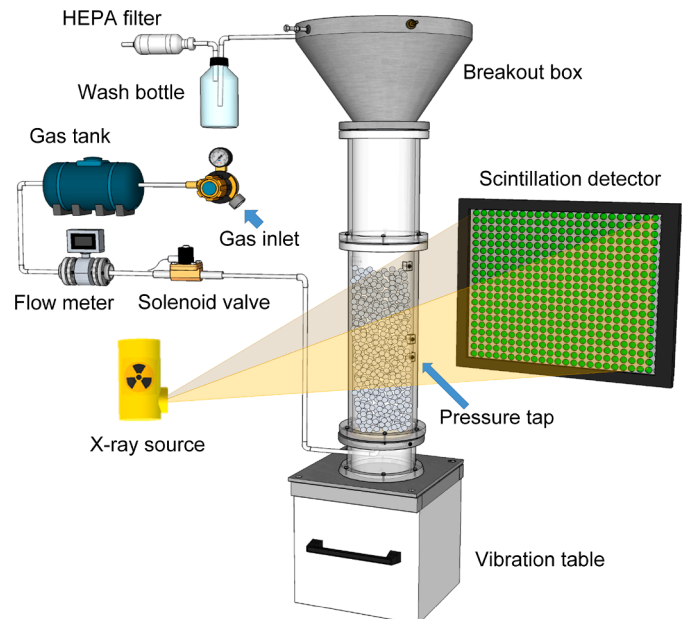


Fig. 1. Schematic representation of the experimental setup.

2.2. Oscillatory gas flow

Oscillatory gas flow was generated at a pressure of 4 bar using a gas flow system that comprises a flow meter, a 2 L gas reservoir, and a solenoid valve (MKS 154B type). This valve was controlled by the LabVIEW panel to produce an oscillatory pulsed flow. A fast-response flow meter (OMEGA FMA-1611A), calibrated with a Bronkhorst mass flow controller (F-202AV), was employed to regulate the pulsed flows. In the prior studies, it was demonstrated that vibration can effectively eliminate gas channeling at a superficial gas velocity of 1.8 cm s^{-1} (Wu et al., 2023a; Kamphorst et al., 2024a). To ensure consistency and facilitate comparisons across various assistance methods, the mean velocity, M , was maintained at 1.8 cm s^{-1} for all experiments. The inlet pulsed superficial gas velocity, U_0 , was configured in a sinusoidal pattern:

$$U_0 = M + A \cdot \sin(2\pi f t) \quad (1)$$

where A and M are the amplitude and the mean flow velocity of the applied oscillatory flow, respectively, and f denotes the oscillating flow frequency. Experiments under various pulsed flow conditions, as detailed in Table 1. The effect of varying pulse conditions on the superficial gas velocity, particularly the volume of gas injected per pulse, is illustrated schematically in Fig. 2.

2.3. Powder properties

Geldart C silica powder (CWK Bad Köstritz) was used in the experiments. The primary particle size distribution was determined using a Malvern 3000 particle size analyzer, operating in a dry powder module. In the measurement, the powder is dispersed by accelerating it through the high-energy Venturi at 4.0 bar, which generates controlled shear forces that separate particles, promoting the formation of a stable dispersion suitable for accurate PSD analysis. This process effectively breaks up agglomerates, ensuring that individual particles are measured. This analysis revealed a monomodal volume-based distribution with a Sauter mean diameter d_{32} of $7.9 \mu\text{m}$, as displayed in Fig. 3. Additionally, a scanning electron microscopy (SEM) image of the untreated powder is included in the figure appended to Fig. 3, showing that the attained PSD closely aligns with the sizes observed by SEM. The silica powder is characterized by its porous nature and possesses a particle density of 1900 kg/m^3 .

In a previous study using the same powder, it was demonstrated that the gas channels remain in the powder bed up to a superficial gas velocity of 7.0 cm s^{-1} in the absence of assistance methods (Kamphorst et al., 2024b). This complicates the experimental determination of the minimum fluidization velocity, U_{mf} , associated with unassisted fluidization. The bulk density of the powder is 134 kgm^3 obtained by filling a measuring column with untreated powder without any compaction. The cohesive nature of the silica powder results in the formation of agglomerates upon interaction during fluidization. The dynamic angle of repose, measured at 50° with a drum rotating at 30 rpm, is indicative of poor flowability as per the Carr classification (Beakawi Al-Hashemi and Baghabra Al-Amoudi, 2018).

2.4. X-ray imaging procedure

The hydrodynamics of pulsed fluidized beds were assessed using an in-house fast X-ray imaging set-up. This is a non-invasive and hard field technique widely acknowledged for its capability to effectively evaluate

Table 1
Pulsed flow conditions investigated.

Symbol	Parameter	Value
f	pulse frequency (Hz)	0.5, 1.0, 2.0
A	pulse amplitude (cm/s)	0.3, 0.6, 0.9, 1.2
M	mean velocity (cm/s)	1.8

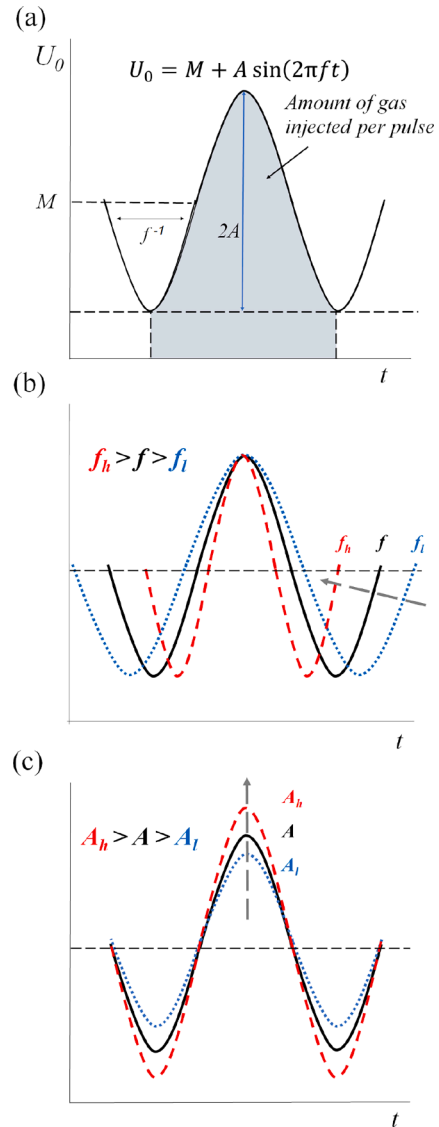


Fig. 2. Schematic representation of the superficial gas velocity U_0 , during one and a half period of the gas pulsation, for a given amplitude, A , and frequency, f . (a) The amount of gas injected in each pulse, with the given sinusoidal flow expression. Illustration of the time interval lengths and the associated gas amount, with variations attributed to (b) f and (c) A .

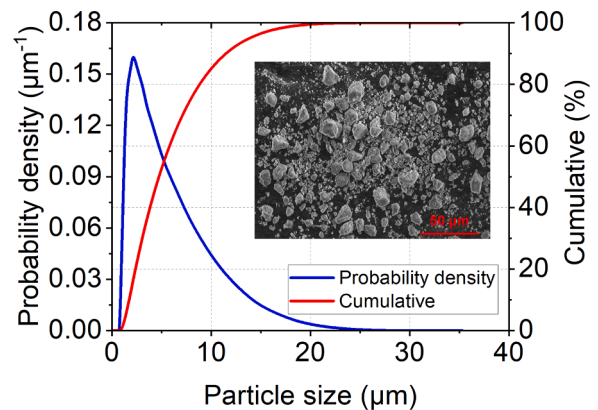


Fig. 3. Volume-based particle size distribution and SEM image of the SiO_2 micropowder.

the hydrodynamics of opaque systems (Bruni et al., 2002; Helmi et al., 2017; Gómez-Hernández et al., 2017). X-ray imaging captures a two-dimensional projection of the three-dimensional pulsed fluidized bed, as depicted in Fig. 1.

The X-ray imaging setup comprised a standard industrial X-ray source (Yxlon International GmbH) operating in cone beam mode, capable of emitting X-rays with a maximum energy of 150 keV. Opposite the X-ray source, a two-dimensional scintillation detector (Teledyne Dalsa Xineos) was positioned. The X-ray source, column and detector were setup in an arrangement that the full width of the column was effectively projected on the detector. The raw X-ray images were acquired at a frame rate of 10 Hz, allowing for detailed temporal analysis of the fluidized bed hydrodynamics.

X-ray beams attenuate when propagating through gas-solid suspensions, which is directly proportional to the mass of solids present along the pathway (Mudde, 2010). During experimentation, the attenuated X-ray beams were measured at the detector plate to construct a two-dimensional intensity map of the field of view. The attenuation of the X-ray beams is considered to follow the Lambert–Beer law (Eq. (2)). A validation study affirmed that even with denser glass beads, the deviation from the Lambert–Beer law due to potential beam hardening is negligible (Ma et al., 2019b).

$$I = I_0 \exp(-\mu d) \quad (2)$$

where I_0 and I are the intensity of X-ray beams before and after penetrating a medium of thickness d , and μ is the attenuation coefficient associated with the material properties.

The gas fraction of the pulsed fluidized bed is derived from the measured intensity profile map. To determine the gas fraction map from the intensity map, a two-point calibration protocol is employed, utilizing two X-ray intensity reference profiles: I_{empty} for an empty column and I_{full} for a fully loaded column. The normalized gas fraction, denoted as ϵ (referred to as gas fraction for simplicity), can be computed. To ensure reproducibility and detect powder compaction during experimentation, the loaded powders in the column were subjected to vibration for a duration of 10 min to attain a close packing state. At time t , the gas fraction ϵ_t of the projection is then calculated using the following expression:

$$\epsilon_t(I) = \frac{\ln(I / I_{\text{full}})}{\ln(I_{\text{empty}} / I_{\text{full}})} \quad (3)$$

The gas fraction at time t , denoted by ϵ_t , is defined to have a range between 0 and 1, representing the close packing of particles at 0 and pure gas at 1. A time-averaged gas fraction profile ϵ can be computed as follows:

$$\epsilon(x, y) = \frac{1}{N_{\Delta t}} \sum_{t=t_0}^{t_0+\Delta t} \epsilon_t(x, y, t) \quad (4)$$

In the gas fraction maps presented in this manuscript, high attenuation of X-rays is visually represented by blue, indicating high solid concentrations. Conversely, low attenuation of X-rays is depicted by red, signifying low solid concentrations within the column.

2.5. Analysis methods of fluidization properties

During the initial phase of fluidization, cohesive powders often form as a plug, which collapses after some time. For consistent comparisons, the onset of fluidization, denoted by $t = 0$, is marked as the instant when the entire powder bed has settled. Both the pulsed flow (and vibration if used) were set to start at this point. Fluidization for each experiment was maintained for 9 min, during which X-ray imaging and pressure drop measurements were conducted.

Pressure series oscillations provide crucial insights into the hydrodynamics of the system. In pulsed beds, these oscillations primarily arise from periodic gas pulsations and subsequent bubbling episodes. The introduction of mechanical vibration also induces periodic oscillations in the bed mass, with a magnitude considerably exceeding those caused

by rising bubbles. Such driven oscillations interfere with the bed pressure drop, complicating the analysis of the fluidization state. To mitigate the disturbance introduced by fluctuations within the system, pressure drop graphs were created using averages of 1000 data points, equivalent to 1.0 s. To further examine the components of such oscillations, signal analysis was performed using both time and frequency domain methodologies (van Ommen et al., 2011; Wu et al., 2023b).

Based on the visualization of 2D flow patterns, gas channels are classified into three types according to their spatial structures and dimensions, that are: vein-like micro-cracks, elongated channels, and wide rat-holes, indicated in red in Fig. 4. The analysis only incorporates elongated channels and rat-holes, which cause substantial gas bypassing. Therefore, the analysis is conducted only for the top section to focus on the major channels and reduce the noise induced by vein-like micro-cracks. For the 2D representation of flow patterns, the images are pretreated using an adaptive threshold method to distinguish between gas-rich areas and gas-lean zones based on gas fraction ϵ . Each pixel is respectively assigned a value of either 1 or 0. These binary images can be averaged over time, obtaining a bubble probability map C_t .

A persistent gas channel structure is identified when the average occurrence of gas-lean areas over 10 s surpasses a probability threshold of 0.6. This criterion ensures that moving bubbles are excluded from the gas channel analysis. For the details of how gas channels are detected and analyzed, we refer to the illustrative examples provided in the Supplementary Material. Furthermore, channels originating from the bottom boundary of the upper section are presumed to arise from the distributor. The captured channels are subsequently characterized based on their major and minor axis lengths, referred to channel length and width, respectively. For each condition, a kernel density estimation is conducted on all channelling events captured, aiming to evaluate the effects of different pulsation modes on the major and minor axis lengths.

The stability of gas channels is assessed by cross-correlating channel states captured with intervals of 5.0 s and time-averaged over 1 s, which is found sufficient for distinguishing differences while excluding transient gas bubbles. The similarity, denoted as S , between two consecutive time-averaged frames, C_t and C_{t+1} , is quantified as follows:

$$S = \frac{\sum_{x,y} [(C_{t+1}(x, y) \times C_t(x, y))] }{\sum_{x,y} [(C_t(x, y) \times C_t(x, y))] } \quad (5)$$

The magnitude of S is directly proportional to the similarity between consecutive frames, with a higher S indicating a more stable channeling state. It is worth mentioning that gas channels are detected based on a 2D projection, which may result in an underestimation of channel dimensions when they overlap in the projection direction. The random formation of gas channels and the sufficiently long fluidization help minimize this potential bias. For stability determination, two channel structures are considered correlated if the S value surpasses 0.5.

3. Results and discussion

In this section, a comparative analysis that examines the effects of various gas pulsation configurations and their combination with mechanical vibration on fluidization is provided. This evaluation focuses on critical fluidization properties, such as flow patterns, gas channel formation, and variations in pressure drop, aiming to provide insights into the optimal conditions for minimizing poor fluidization behavior, such as gas channeling and uneven gas distribution.

3.1. Hydrodynamics of unassisted, pulsed and vibrated fluidized beds

Fig. 4 illustrates the distinct fluidization states observed in unassisted, vibrated, and pulsed fluidized beds upon achieving a steady fluidization state. In absence of any assistance, micro-silica particles initially cluster together, forming a plug that ascends within the column. Upon reaching the breakout box, the plug disintegrates, and the particles

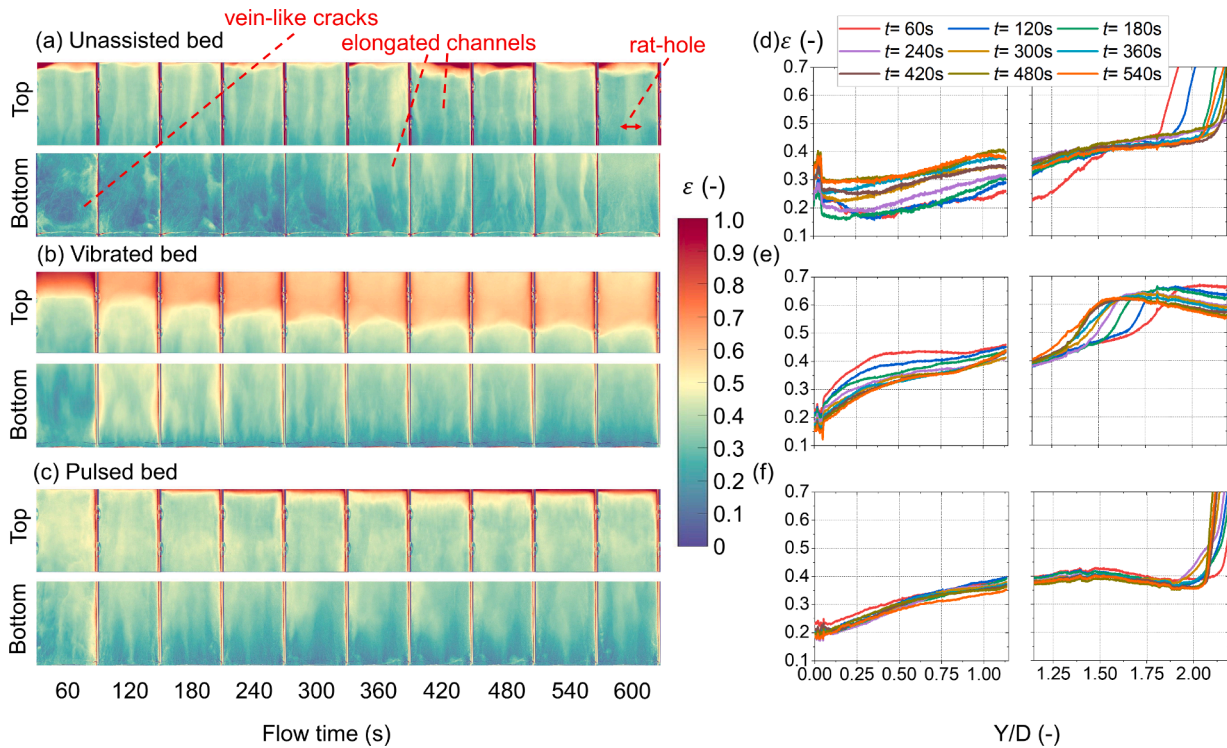


Fig. 4. Time-averaged flow patterns in the (a) unassisted, (b) vibrated and (c) pulsed fluidized beds. The gas fraction profiles in the vertical direction for each respective case are shown in subfigures (d), (e) and (f). Each flow pattern is obtained by averaging 2 s of frames at each selected time. $U_0 = 1.8 \text{ cm s}^{-1}$; $f_v = 30 \text{ Hz}$; $A_v = 1 \text{ mm}$; $A = 0.9 \text{ cm s}^{-1}$, $f = 0.5 \text{ Hz}$, $D = 19.2 \text{ cm}$.

descend and reassemble on the distributor plate. A comprehensive analysis of this slugging behavior is described in Kamphorst et al. (2024a). The resulting settling process yields a moderately dilated powder bed characterized by random vein-like cracks and elongated gas channels. The bed pressure drop for unassisted fluidization, as displayed in Fig. 5, also indicates that a substantial portion of the bed material remains defluidized due to channeling behavior. As shown in Fig. 4a, these gas channels gradually develop and extend to the upper section of the bed. Nevertheless, this configuration of multiple channels is inherently unstable; over time, the channels tend to coalesce into a single ‘rat-hole’, which occupies a substantial portion of the bed. This configuration allows a considerable volume of gas to bypass the bed material, resulting in poor fluidization.

Mechanical vibration effectively suppresses the formation of elongated channels and rat-holes, as shown in Fig. 4b. Such an effect is also reflected in the normalized pressure drop data shown in Fig. 5, where a relatively high pressure drop is identified, with an average of 0.985. However, instead of promoting bed expansion and bubbling, vibration induces powder stratification, leading to the emergence of distinct flow regions. It is important to note that the red color appearing at the top of the frame does not correspond to the bed surface; instead, it represents a highly diluted fluidized region. The bottom layer of powder progressively compacts against the vibrating distributor plate, developing a densely packed configuration. Consequently, the dilute phase in the upper section diminishes, resulting in a state of partial fluidization. Our recent work shows that a significant fraction, over half of the powder, remains in this densely packed layer without achieving effective fluidization (Wu et al., 2023a).

Fig. 4c shows greater mitigation of gas channels in the bed operated with a pulsed flow compared to the unassisted bed. Although it is observed that gas channels are not entirely eliminated, their continuous disruption and reformation improve the circulation of the adjacent powder. As the gas flow rate peaks, bubbles are nucleated. Unlike the homogeneous distribution of bubbles typically observed in a Geldart A

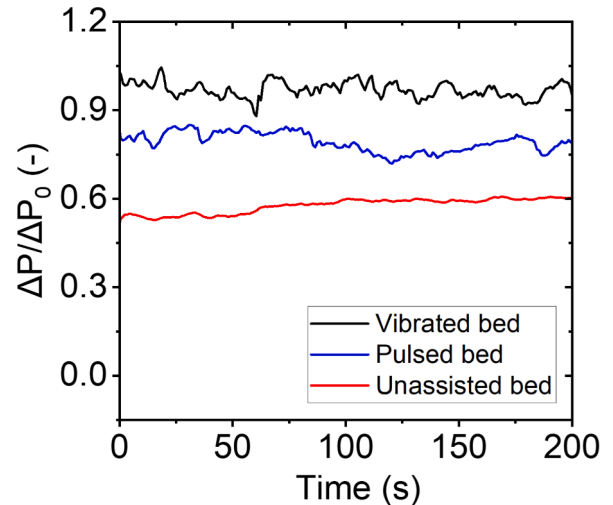


Fig. 5. Normalized pressure data of vibro-, pulsed and unassisted fluidized beds. $U_0 = 1.8 \text{ cm s}^{-1}$; $f_v = 30 \text{ Hz}$; $A_v = 1 \text{ mm}$; $A = 0.9 \text{ cm s}^{-1}$, $f = 0.5 \text{ Hz}$, $D = 19.2 \text{ cm}$. The pressure drop is normalized by the static pressure.

particle bubbling bed, bubbles in pulsed beds frequently relocate alongside gas channels, resembling the dynamic characteristics of a spouted bed. Therefore, the solid mixing rate in pulsed beds is expected to fall in between that of unassisted and vibrated beds.

3.2. Effect of pulsation frequency

The effect of gas pulsation on the fluidization of cohesive silica diminishes as the pulse frequency is increased. As illustrated in Fig. 6, there is no substantial variation in bed expansion (shown by the red front appearing at the top of the columns) and gas fraction across varied

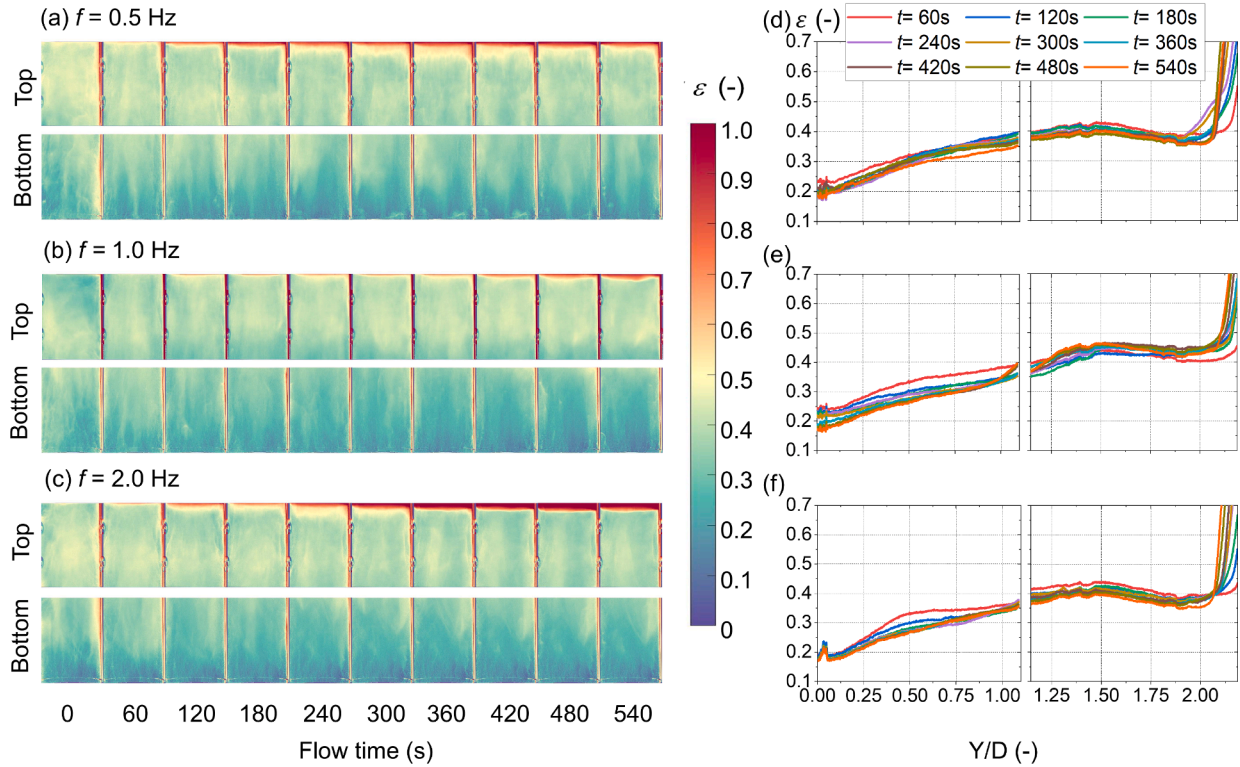


Fig. 6. Time-averaged flow patterns in the pulsed fluidized beds with varying pulsation frequency of (a) 0.5 Hz, (b) 1.0 Hz and (c) 2.0 Hz. The gas fraction profiles for each respective case are shown in (d) - (f). Each flow pattern is obtained by averaging 2 s of frames at each selected time to reduce noise. $M = 1.8 \text{ cm s}^{-1}$; $A = 0.9 \text{ cm s}^{-1}$.

frequencies, which shows a comparable degree of bed dilation. Sending pulsations in such rapid succession at high frequencies causes the pulses to merge into one another, thereby mitigating their disruptive effect on gas channels and resulting in diminished solids mixing in the lower section relative to the upper section. Across all tested frequencies, persistent gas channels tend to form in the lower bed section over time, while the upper bed experiences more pronounced solid mixing and bubbling. Fig. 6 shows that pulsating the bed at frequencies of 0.5 Hz and 1.0 Hz tends to suppress gas channeling more effectively (see Video S1 in the Supplementary Material). Nevertheless, it is worth noting that while these channels are not entirely eliminated, the structures reform approximately every 20 s. In contrast, higher pulse frequencies, such as 2.0 Hz, are less effective in disrupting channels, and results in an extended stable time of the channels, t_c , often exceeding 40 s, resembling the flow behavior observed in unassisted beds. A summary of average channel stable time is provided in Table 2.

In addition to effectively disrupting gas channels, low-frequency gas pulsations are found to be capable of suppressing elongated channels. As shown in Fig. 7, channels at 0.5 Hz and 1.0 Hz primarily exhibit major lengths less than $0.7D$. In addition, Fig. 7c reveals that channels appear more extended at 2.0 Hz, indicating the less effective pulsation. In the absence of any assistance, long gas channels start to form and persist, reaching lengths close to $1.2D$. Furthermore, low-frequency pulsation reduces the emergence of persistent channels. Fig. 8 shows that pulsation at 0.5 Hz and 1.0 Hz induces rapid channel modifications in channel structure, consequently shortening the stable time of channels. At higher frequencies like 2.0 Hz, persistent channels are notably prevalent, with the flow pattern similarity S consistently above 0.5.

Collectively, the bed behaviors tell that intermittent bubbling plays a crucial role in disrupting gas channels. At each pulse peak, some channels become discontinuous, forming a bubble train. The pulsation lifts the bottom powder and disrupts the gas channels by temporarily exceeding their maximum stable gas throughput. As the gas flow rate decreases during the second half of the cycle, the gas channels tend to reappear

Table 2

Average stable channel time t_c for the experiments with various pulse frequencies and amplitudes.

f (Hz)	A (cm/s)	t_c (s)
0.5	0.3	38.5
0.5	0.6	20.0
0.5	0.9	16.3
0.5	1.2	74.0
1.0	0.9	15.2
2.0	0.9	39.6

with the contraction of the bed. Such an effect is more pronounced at 0.5 Hz. When the pulsation frequency is increased, the volume of gas injected per pulse reduces, as illustrated in Fig. 2, causing the pulses to dissipate more easily. Consequently, at a higher frequency, the pulses become insufficient to alter the flow behavior, allowing the gas channels to more readily withstand the stimulation.

Additionally, variations in powder bed depth and size may lead to different trends observed in the effect of pulsation frequency compared to the results shown above. Further experiments conducted in a column with a diameter of 9.0 cm are provided in the Supplementary Materials.

The normalized pressure drops of the powder bed subjected to flow pulsations of various frequencies are displayed in Fig. 9. The data demonstrate that the normalized pressure drop is approximately 0.8, regardless of the pulse frequency. This value is considerably higher than the plateau of 0.6 observed for unassisted fluidization. However, based on pressure drop alone, it cannot be concluded whether a homogeneous bed is achieved.

Furthermore, a Fourier transform of the obtained pressure data is provided in Fig. 10. As expected, primary peaks are located at the frequency of pulsation. Additionally, harmonic peaks appear at multiples of the pulse frequency. The insets display the pulse signal as measured at the top and bottom of the column, where the 'bottom' spans from the distributor plate to $H = 1.43D$, and the 'top' runs from $H = 1.43D$

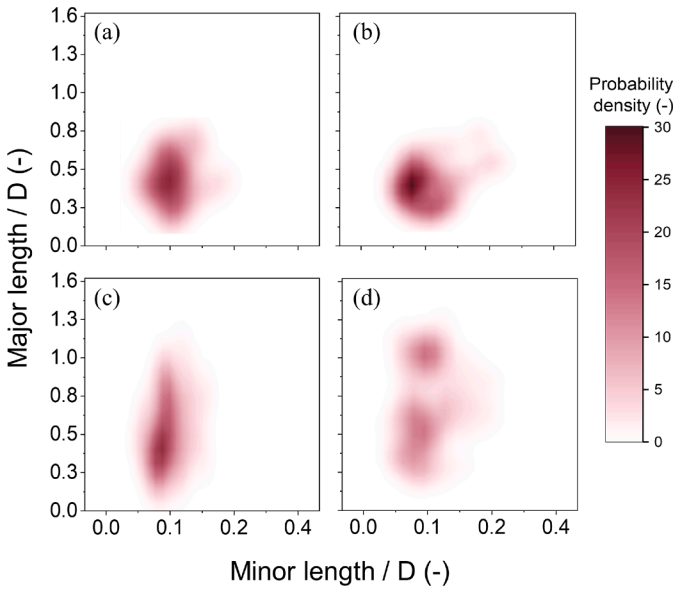


Fig. 7. Kernel density estimation on gas channels captured in the upper section of the pulsed fluidized beds with varying pulsation frequency of (a) 0.5 Hz, (b) 1.0 Hz, (c) 2.0 Hz and (d) the unassisted fluidized bed. $M = 1.8 \text{ cm s}^{-1}$; $A = 0.9 \text{ cm s}^{-1}$ for the pulsed beds.

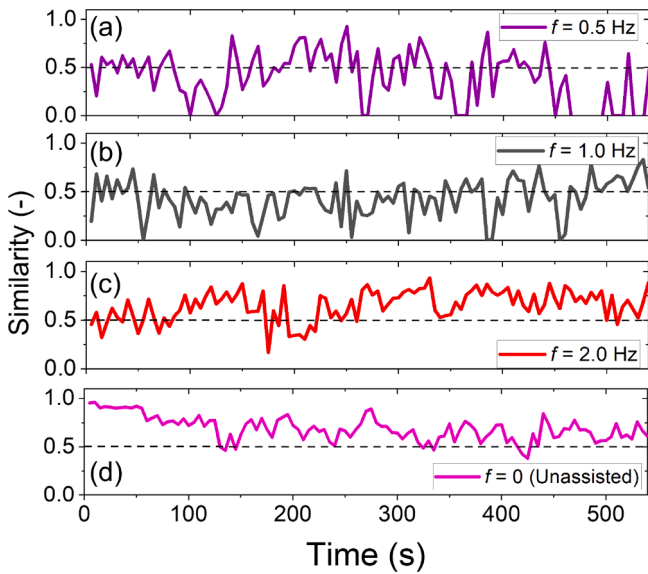


Fig. 8. Similarity of gas channels captured in the upper section of the pulsed fluidized beds with varying pulsation frequency of (a) 0.5 Hz, (b) 1.0 Hz, (c) 2.0 Hz and (d) the unassisted fluidized bed. $M = 1.8 \text{ cm s}^{-1}$; $A = 0.9 \text{ cm s}^{-1}$ for the pulsed beds.

to the breakout box. It was observed that the magnitude of these signals is higher at the bottom compared to the top of the bed, showing significant attenuation of the signal through the powder bed. The oscillations within the bed provided by the gas flow induce a non-homogeneous pressure profile. As the fluctuations are more pronounced in the bottom of the bed, larger pressure differences within one pulse are experienced there. These introduce a driving force for the pulse amplitude to flatten while the gas is rising through the bed, leading to less consistent oscillations in the top of the bed, explaining the observed attenuation. This finding concerns a possible limitation in the context of scaling the pulsed flow assistance method. Provided that the pulse loses potency along column height, limited benefits can be attained from applying this technique to tall beds.

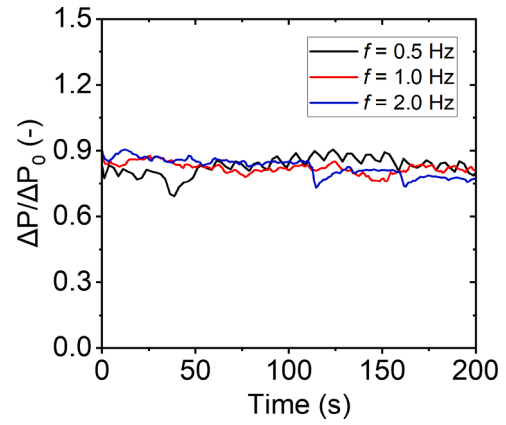


Fig. 9. Normalized pressure drop of fluidized beds assisted with pulsed flow at various frequencies. $M = 1.8 \text{ cm s}^{-1}$, $A = 0.9 \text{ cm s}^{-1}$.

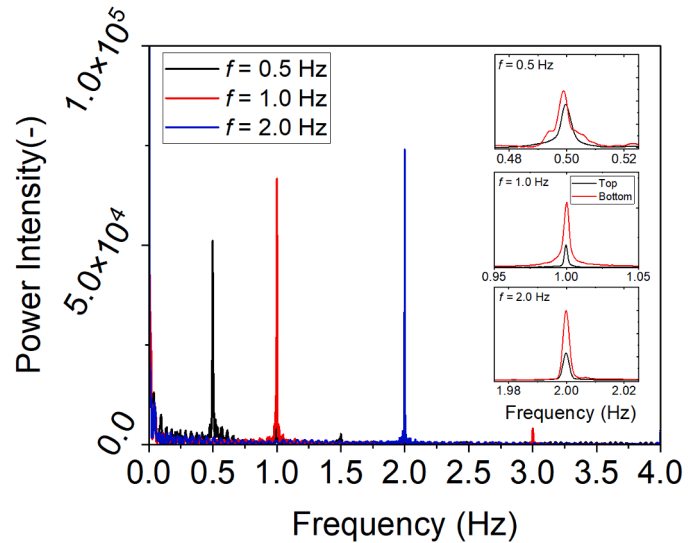


Fig. 10. Fourier transform of pressure signals measured in beds subjected to pulsed flow of various frequencies. The insets display signals measured just above the distributor plate and in the top of the bed.

3.3. Effect of pulsation amplitude

The pressure drop data corresponding to the experiments performed at varying pulse amplitudes, shown in Fig. 11, demonstrate an optimal amplitude range of 0.6 to 0.9 cm s^{-1} with respect to fluidized fraction. The comparatively low pressure drops observed at 0.3 and 1.2 cm s^{-1} suggest the presence of channeling or otherwise defluidized fractions within the bed.

Fig. 13 shows that pulse amplitude has a significant impact on the effectiveness of gas pulsation in disrupting gas channels (also see Video S2 in the Supplementary Material). A reduction in pulse amplitude leads to reduced channel rearrangement. In particular, at an amplitude of $A = 0.3 \text{ cm s}^{-1}$, the gas pulse is ineffective in disrupting the channels. Subsequently, the flow pattern reaches a steady state after $t = 240 \text{ s}$, with no further alterations observed.

The most effective suppression of gas channels is observed at moderate pulse amplitudes. As demonstrated in Fig. 13, the minimal channel length manifests at amplitudes of $A = 0.6$ and 0.9 cm s^{-1} . Under these amplitudes, the gas channels predominantly appear with a dimension of $0.5D$, which is more pronounced compared to other amplitude conditions. This indicates the presence of shorter channels within the bed and enhances the distribution of bubbles.

Upon increasing the amplitude to 1.2 cm s^{-1} , the system quickly reached a stable state with a rat-hole forming in the center of the bed

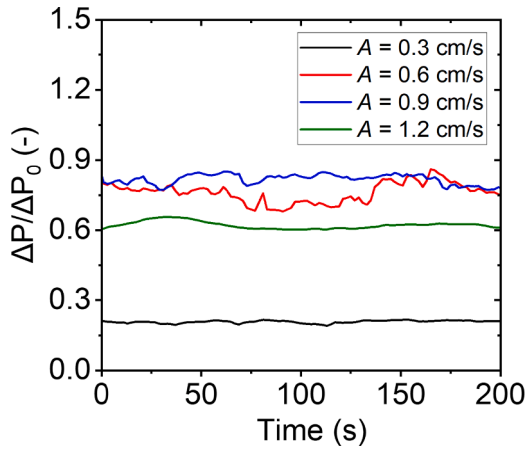


Fig. 11. Normalized pressure data of fluidized beds assisted with pulsed flow at various amplitudes. $M = 1.8 \text{ cm s}^{-1}$, $f = 0.5 \text{ Hz}$. The pressure drop is normalized by the static pressure.

within the initial 60 s, as shown in Fig. 12. This phenomenon is postulated to arise from the interplay of a substantial pulsation amplitude and a diminished offset value. The increased amplitude necessitates broader channels to accommodate the increased flow throughout each cycle. Simultaneously, the excessively low minimum flow rate leads to a pronounced contraction of the bed, significantly defluidizing the powder and limiting the disruption of gas channels. This results in the establishment of a robust powder structure that persists for the remaining fluidization time. Fig. 13 illustrates that the length of the gas channels

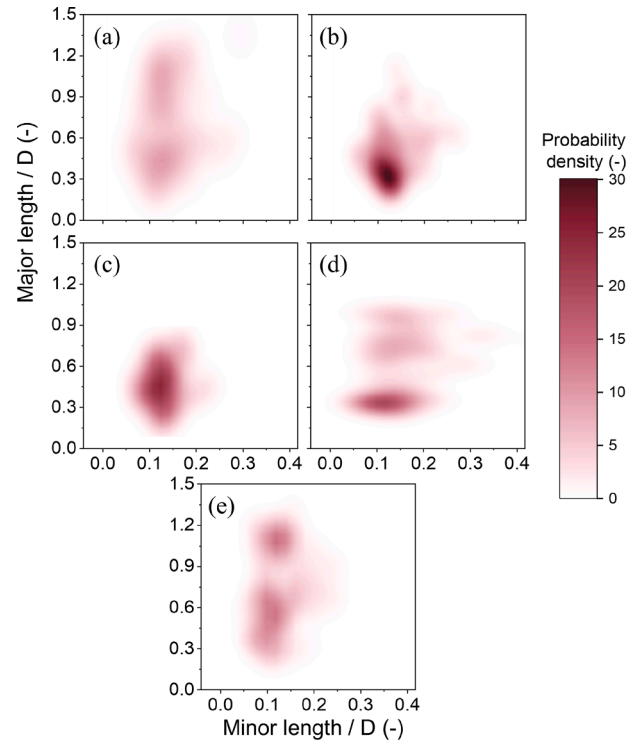


Fig. 13. Kernel density estimation on gas channels captured in the upper section of the pulsed fluidized beds with varying pulsation amplitude of (a) $A = 0.3 \text{ cm s}^{-1}$, (b) $A = 0.6 \text{ cm s}^{-1}$, (c) $A = 0.9 \text{ cm s}^{-1}$ and (d) $A = 1.2 \text{ cm s}^{-1}$, and (e) the unassisted fluidized bed. $M = 1.8 \text{ cm s}^{-1}$; $f = 0.5 \text{ Hz}$ for the pulsed beds.

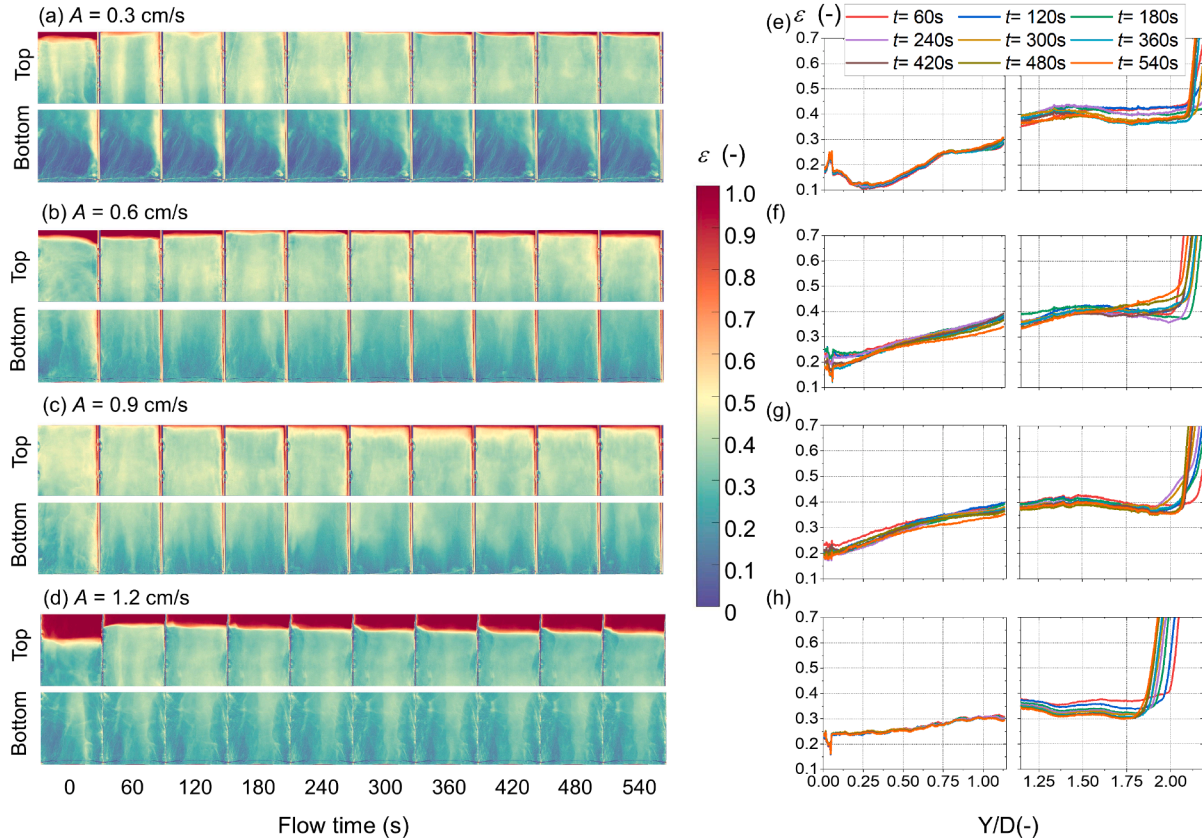


Fig. 12. Time-averaged flow patterns in the pulsed fluidized beds with varying pulsed velocity of (a) $A = 0.3 \text{ cm s}^{-1}$, (b) $A = 0.6 \text{ cm s}^{-1}$, (c) $A = 0.9 \text{ cm s}^{-1}$ and (d) $A = 1.2 \text{ cm s}^{-1}$. The gas fraction profiles for each respective case are shown in (e) - (h). Each flow pattern is obtained by averaging 2 s of frames at each selected time to reduce noise. $M = 1.8 \text{ cm s}^{-1}$, $f = 0.5 \text{ Hz}$.

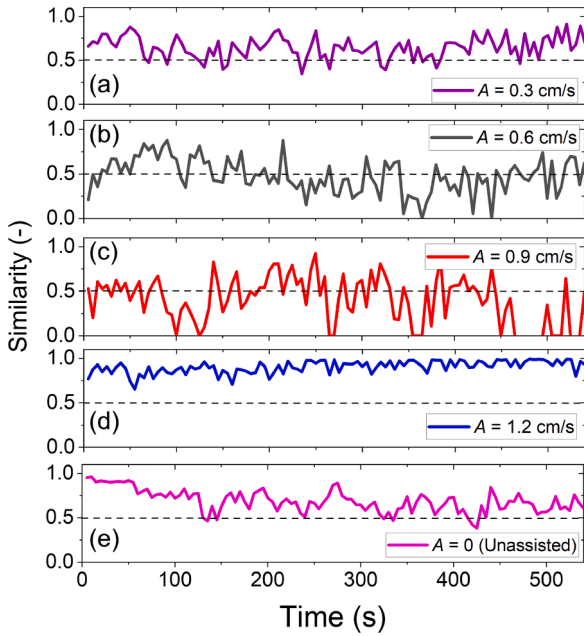


Fig. 14. Similarity of gas channels captured in the upper section of the pulsed fluidized beds with varying pulsation frequency of (a) $A = 0.3 \text{ cm s}^{-1}$, (b) $A = 0.6 \text{ cm s}^{-1}$, (c) $A = 0.9 \text{ cm s}^{-1}$ and (d) $A = 1.2 \text{ cm s}^{-1}$, and (e) the unassisted fluidized bed. $M = 1.8 \text{ cm s}^{-1}$; $f = 0.5 \text{ Hz}$ for the pulsed beds.

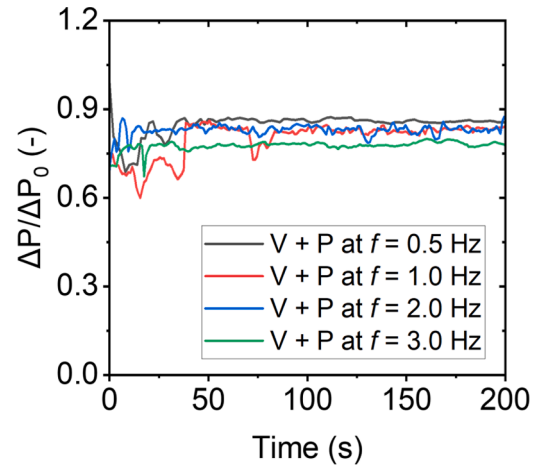


Fig. 16. Normalized pressure data of fluidized beds assisted with pulsed flow at various frequencies with vibration. $M = 1.8 \text{ cm s}^{-1}$; $A = 0.9 \text{ cm s}^{-1}$; $f_v = 30 \text{ Hz}$; $A_v = 1 \text{ mm}$. The pressure drop is normalized by the static pressure. In the legend, abbreviation V stands for vibration, and P presents pulsation.

is approaching $1.0D$, extending up to the bed surface due to the diminished bed expansion. Consequently, the long channels are not suppressed under such pulsation conditions. The most rapid-changing flow patterns are identified at $A = 0.6 \text{ cm s}^{-1}$ and $A = 0.9 \text{ cm s}^{-1}$, with some episodes where the similarity S drops to zero. In contrast, at an amplitude of $A = 1.2 \text{ cm s}^{-1}$, the gas-solids distribution shows little variation, with minimal disruption to the channel configuration, as indicated in Fig. 14.

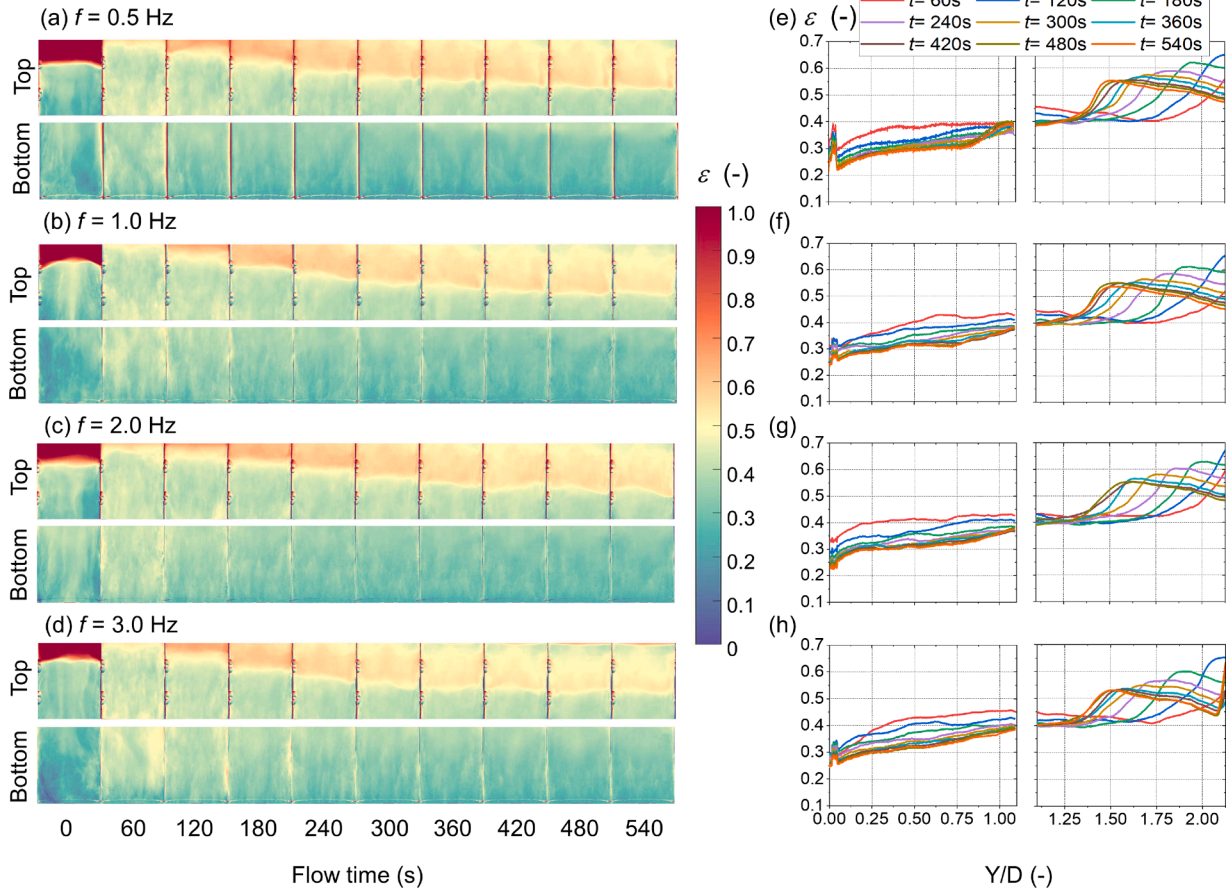


Fig. 15. Time-averaged flow patterns in the vibro-pulsed fluidized beds with varying pulsation frequency of (a) 0.5 Hz, (b) 1.0 Hz, (c) 2.0 Hz and (d) 3.0 Hz. The gas fraction profiles for each respective case are shown in (e)–(h). Each flow pattern is obtained by averaging 2 s of frames at each selected time to reduce noise. $M = 1.8 \text{ cm s}^{-1}$; $A = 0.9 \text{ cm s}^{-1}$; $f_v = 30 \text{ Hz}$; $A_v = 1 \text{ mm}$.

3.4. Effect of combined pulsation and vibration

Both pulsation and vibration assistance methods exhibit different limitations, but a synergistic effect between the two methods could provide effective assistance for the fluidization of cohesive powders. When a pulsed flow is superimposed onto a vibrated bed, long gas channels are completely suppressed, as observed in Fig. 15. The flow patterns are characterized by vigorous bubbling in the upper section and intermittent bubbling occurring at the pulsation frequency in the lower section. Despite the effect of pulsation, the stratification of different flow regions—a characteristic observed in vibrated beds of cohesive powder—remains evident (Wu et al., 2023a).

Remarkably, in the presence of mechanical vibration, no discernible difference in fluidization behavior is observed when utilizing pulsed flow operation at various frequencies. Fig. 15 demonstrates how the stratification front between the dilute and dense phases propagates. The stratification front consistently descends to $Y/D = 1.50$ across all the pulsation frequencies at $t = 540$ s, consistent with the observations in the vibrated bed without pulsation, as shown in Fig. 4b. This result indicates that the pulsation slightly delays the stratification process, but does not prevent it. Additionally, the gas fraction in the upper section is also observed to be lower than in the vibrated-only bed, which is attributed to the intermittent bubbling induced by the periodic pulsation.

Pulsation is capable of modifying the dense region at the bottom of the bed. As illustrated in Figs. 4b and 15, the bottom section appears less dense in beds subjected to both vibration and pulsation compared to those influenced solely by vertical vibration. Despite the periodic pulsation resulting in less vigorous bubbling, especially within the dense region ($Y/D < 0.5$), it introduces a periodic gas wave that permeates the compact powder structure in the bottom section. This counteracts the consolidation effects due to the interaction between the vibration plate and the powder. However, stratification continues to prevail in the fluidization process, and the overall fluidization process is largely governed by vibrational assistance. It is worth noting that the impact of pulsation diminishes as it progresses to the upper section, as shown in Fig. 10. Therefore, different effects can be anticipated in the bottom and top sections of the bed.

The normalized pressure drops under various pulsation frequencies combined with mechanical vibration are presented in Fig. 16. Compared to pulse-assistance alone shown in Fig. 9, the addition of vibration generally increases the pressure drop. The highest normalized pressure drop, averaging 0.852, is observed at $f = 0.5$ Hz, slightly higher than the value of approximately 0.818 observed for pulsation alone, indicating an improvement in fluidization.

4. Conclusions

The study presents a comprehensive comparison of the effects of gas pulsations on the fluidization of cohesive powder, investigating varying frequencies and amplitudes with and without mechanical vibration in a relatively large lab-scale fluidized bed column ($D = 19.2$ cm). X-ray imaging technique provides direct insights into the flow patterns. Different from the Geldart A/B particles, where periodic pulsation enhances the fluidization by promoting homogeneous and ordered flow structures (Wu et al., 2025), the experimental results reveal that, for cohesive Geldart C powder, gas pulsation frequently disrupts long gas channels, thereby improving solids circulation and aeration. Nevertheless, the formation of gas channels is not completely suppressed, preventing the bed from achieving a fully fluidized state. Introducing gas pulsation to a mechanically vibrated bed reveals a minimal effect on fluidization. While pulsation is demonstrated to mitigate solid compaction at the bottom of the bed, the flow pattern is observed to be dominated by the effects of vibration, with stratification continuing to prevail.

Experimental studies employing powders of varying cohesiveness—quantified through measurements such as atomic forces or agglom-

eration tests—could provide valuable insights into the mechanisms underpinning the observed phenomena. Given the observed stability of channels and the dampening effect of gas pulsation by the bed material, gas pulsation alone is believed to be sub-optimal for scale-up practices. More vigorous agitation or impact applied to the powder may be required. Other assistance methods, or combinations thereof—such as mechanical vibration and stirring—appear to show greater promise for enhancing the fluidization of cohesive powders. Pulsation could be beneficial in terms of overcoming drawbacks, such as solid compaction and the formation of dead zones, when applied simultaneously with other methods.

Data availability

Data will be made available on request.

Declaration of competing interest

The authors declare that they have no known competing financial interests or personal relationships that could have appeared to influence the work reported in this paper.

CRediT authorship contribution statement

Kaiqiao Wu: Writing – review & editing, Writing – original draft, Visualization, Supervision, Methodology, Investigation, Funding acquisition, Formal analysis, Data curation, Conceptualization; **Rens Kamphorst:** Writing – original draft, Validation, Investigation, Formal analysis, Data curation; **P. Christian van der Sande:** Writing – original draft, Visualization, Validation, Investigation, Formal analysis; **Evert C. Wagner:** Writing – review & editing, Methodology, Investigation; **Gabrie M.H. Meesters:** Writing – review & editing, Supervision, Project administration, Methodology, Funding acquisition, Conceptualization; **J. Ruud van Ommen:** Writing – review & editing, Supervision, Project administration, Methodology, Funding acquisition, Conceptualization.

Acknowledgments

The authors would like to acknowledge Stefan ten Hagen for his contribution on the development of the fluidized bed reactor.

This work received funding from the Dutch Research Council (NWO) in the framework of the ENW PPP Fund for the top-sectors (741.019.202) and from the Ministry of Economic Affairs in the framework of the “PPS-Toeslageregeling” (2020.023.A.TUD.1). This work was also supported by the National Natural Science Foundation of China (52406181).

Supplementary material

Supplementary material associated with this article can be found in the online version at [10.1016/j.ces.2025.121529](https://doi.org/10.1016/j.ces.2025.121529).

References

- Akhavan, A., van Ommen, J.R., Nijenhuis, J., Wang, X.S., Coppens, M.-O., Rhodes, M.J., 2008. Improved drying in a pulsation-assisted fluidized bed. *Ind. Eng. Chem. Res.* 48 (1), 302–309. <https://doi.org/10.1021/ie800458h>
- Akhavan, A., Rahman, F., Wang, S., Rhodes, M., 2015. Enhanced fluidization of nanoparticles with gas phase pulsation assistance. *Powder Technol.* 284, 521–529. <https://doi.org/10.1016/j.powtec.2015.07.004>
- Al-Ghurabi, E.H., Shahabuddin, M., Kumar, N.S., Asif, M., 2020. Deagglomeration of ultra-fine hydrophilic nanopowder using low-frequency pulsed fluidization. *Nanomaterials* 10 (2). <https://doi.org/10.3390/nano10020388>
- Alavi, S., Caussat, B., 2005. Experimental study on fluidization of micronic powders. *Powder Technol.* 157 (1), 114–120. <https://doi.org/10.1016/j.powtec.2005.05.017>
- Ali, S.S., Arsad, A., Asif, M., 2021. Effect of modified inlet flow strategy on the segregation phenomenon in pulsed fluidized bed of ultrafine particles: a collapse bed study. *Chem. Eng. Process.* 159, 108243. <https://doi.org/10.1016/j.cep.2020.108243>
- Ali, S.S., Asif, M., 2012. Fluidization of nano-powders: effect of flow pulsation. *Powder Technol.* 225, 86–92. <https://doi.org/10.1016/j.powtec.2012.03.035>

- Ammendola, P., Chirone, R., 2010. Aeration and mixing behaviours of nano-sized powders under sound vibration. *Powder Technol.* 201 (1), 49–56. <https://doi.org/10.1016/j.powtec.2010.03.002>
- Beakawi Al-Hashemi, H.M., Baghabra Al-Amoudi, O.S., 2018. A review on the angle of repose of granular materials. *Powder Technol.* 330, 397–417. <https://doi.org/10.1016/j.powtec.2018.02.003>
- Bruni, G., Solimene, R., Marzocchella, A., Salatino, P., Yates, J.G., Lettieri, P., Fiorentino, M., 2002. Self-segregation of high-volatile fuel particles during devolatilization in a fluidized bed reactor. *Powder Technol.* 128 (1), 11–21. [https://doi.org/10.1016/S0032-5910\(02\)00149-3](https://doi.org/10.1016/S0032-5910(02)00149-3)
- Chirone, R., Raganati, F., Ammendola, P., Barletta, D., Lettieri, P., Poletto, M., 2018. A comparison between interparticle forces estimated with direct powder shear testing and with sound assisted fluidization. *Powder Technol.* 323, 1–7. <https://doi.org/10.1016/j.powtec.2017.09.038>
- Grace, J.R., 2020. *Introduction, History, and Applications*. John Wiley & Sons, Ltd. chapter 1. pp. 1–9.
- Gómez-Hernández, J., Sánchez-Delgado, S., Wagner, E., Mudde, R.F., van Ommen, J.R., 2017. Characterization of TiO₂ nanoparticles fluidization using X-ray imaging and pressure signals. *Powder Technol.* 316, 446–454. <https://doi.org/10.1016/j.powtec.2016.11.068>
- Helmi, A., Wagner, E.C., Gallucci, F., van Sint Annaland, M., van Ommen, J.R., Mudde, R.F., 2017. On the hydrodynamics of membrane assisted fluidized bed reactors using X-ray analysis. *Chem. Eng. Process.* 122, 508–522. <https://doi.org/10.1016/j.cep.2017.05.006>
- Iannello, S., Foscolo, P.U., Materazzi, M., 2022. Investigation of single particle devolatilization in fluidized bed reactors by X-ray imaging techniques. *Chem. Eng. J.* 431, 133807. <https://doi.org/10.1016/j.cej.2021.133807>
- Ireland, E., Pitt, K., Smith, R., 2016. A review of pulsed flow fluidisation; the effects of intermittent gas flow on fluidised gas solid bed behaviour. *Powder Technol.* 292, 108–121. <https://doi.org/10.1016/j.powtec.2016.01.018>
- Jia, D., Bi, X., Lim, C.J., Sokhansanj, S., Tsutsumi, A., 2016. Biomass drying in a pulsed fluidized bed without inert bed particles. *Fuel* 186, 270–284. <https://doi.org/10.1016/j.fuel.2016.08.100>
- Kamphorst, R., van der Sande, P.C., Wu, K., Wagner, E.C., David, M.K., Meesters, G. M.H., van Ommen, J.R., 2024a. The mechanism behind vibration assisted fluidization of cohesive micro-silica. *KONA Powder Part. J.*, 2024007. <https://doi.org/10.14356/kona.2024007>
- Kamphorst, R., Wu, K., van Baarlen, M., Meesters, G.M.H., van Ommen, J.R., 2024b. Effect of vibrational modes on fluidization characteristics and solid distribution of cohesive micro- and nano-silica powders. *Chem. Eng. Sci.* 291, 119911. <https://doi.org/10.1016/j.ces.2024.119911>
- Kamphorst, R., Wu, K., Salameh, S., Meesters, G. M.H., van Ommen, J.R., 2023. On the fluidization of cohesive powders: differences and similarities between micro- and nano-sized particle gas-solid fluidization. *Can. J. Chem. Eng.* 101 (1), 227–243. <https://doi.org/10.1002/cjce.24615>
- Khosravi Bizhaem, H., Basirat Tabrizi, H., 2013. Experimental study on hydrodynamic characteristics of gas-solid pulsed fluidized bed. *Powder Technol.* 237, 14–23. <https://doi.org/10.1016/j.powtec.2013.01.001>
- Liu, Y., Ohara, H., Tsutsumi, A., 2017. Pulsation-assisted fluidized bed for the fluidization of easily agglomerated particles with wide size distributions. *Powder Technol.* 316, 388–399. <https://doi.org/10.1016/j.powtec.2016.12.049>
- Ma, J., van Ommen, J.R., Liu, D., Mudde, R.F., Chen, X., Pan, S., Liang, C., 2019a. Fluidization dynamics of cohesive Geldart B particles. Part II: pressure fluctuation analysis. *Chem. Eng. J.* 368, 627–638. <https://doi.org/10.1016/j.cej.2019.02.187>
- Ma, J., van Ommen, J.R., Liu, D., Mudde, R.F., Chen, X., Wagner, E.C., Liang, C., 2019b. Fluidization dynamics of cohesive Geldart B particles. Part I: X-ray tomography analysis. *Chem. Eng. J.* 359, 1024–1034. <https://doi.org/10.1016/j.cej.2018.11.082>
- Macrì, D., Sutcliffe, S., Lettieri, P., 2020. Fluidized bed sintering in TiO₂ and coke systems. *Chem. Eng. J.* 381, 122711. <https://doi.org/10.1016/j.cej.2019.122711>
- Mawatari, Y., Hamada, Y., Yamamura, M., Kage, H., 2015. Flow pattern transition of fine cohesive powders in a gas-solid fluidized bed under mechanical vibrating conditions. *Procedia Eng.* 102, 945–951. <https://doi.org/10.1016/j.proeng.2015.01.216>
- Mudde, R.F., 2010. Time-resolved X-ray tomography of a fluidized bed. *Powder Technol.* 199 (1), 55–59. <https://doi.org/10.1016/j.powtec.2009.04.021>
- Nasri Lari, H., Rasouli, M., Chaouki, J., Tavares, J.R., 2020. Solid hold-up measurement in a jet-impactor assisted fluidized bed using gamma-ray densitometry. *AIChE J.* 66 (11), e16653. <https://doi.org/10.1002/aic.16653>
- van Ommen, J.R., King, D.M., Weimer, A., Pfeffer, R., van Wachem, B., Johnson, S., Looije, N., 2013. Experiments and modelling of micro-jet assisted fluidization of nanopowder. In: Knowlton, T., PSRI (Eds.), *10th International Conference on Circulating Fluidized Beds and Fluidization Technology (CFB-10)*, ECI Symposium Series, p. 43.
- van Ommen, J.R., Sasic, S., van der Schaaf, J., Gheorghiu, S., Johansson, F., Coppens, M.-O., et al., 2011. Time-series analysis of pressure fluctuations in gas-solid fluidized beds—A review. *Int. J. Multiph. Flow* 37 (5), 403–428. <https://doi.org/10.1016/j.ijmultiphaseflow.2010.12.007>
- Saayman, J., Nicol, W., van Ommen, J.R., Mudde, R.F., 2013. Fast X-ray tomography for the quantification of the bubbling, turbulent- and fast fluidization-flow regimes and void structures. *Chem. Eng. J.* 234, 437–447. <https://doi.org/10.1016/j.cej.2013.09.008>
- Saidi, M., Basirat Tabrizi, H., Grace, J.R., 2019. A review on pulsed flow in gas-solid fluidized beds and spouted beds: recent work and future outlook. *Adv. Powder Technol.* 30 (6), 1121–1130. <https://doi.org/10.1016/j.apt.2019.03.015>
- van der Sande, P.C., Wu, K., Kamphorst, R., Wagner, E.C., Meesters, G. M.H., van Ommen, J.R., 2025. On the inherent correlation between the fluidization and flow properties of cohesive powders. *AIChE J.*, e18706. <https://doi.org/10.1002/aic.18706>
- Wu, K., Francia, V., Jiang, S., Coppens, M.-O., 2025. An experimental flow regime map to dynamically structure gassolid bubbling fluidized beds. *AIChE J.*, e18681. <https://doi.org/10.1002/aic.18681>
- Wu, K., Wagner, E.C., Ochkin-Koenig, O., Franck, M., Weis, D., Meesters, G. M.H., van Ommen, J.R., 2023a. Time-resolved X-ray study of assisted fluidization of cohesive micron powder: on the role of mechanical vibration. *Chem. Eng. J.* 470, 143936. <https://doi.org/10.1016/j.cej.2023.143936>
- Wu, K., Kamphorst, R., Bakker, A., Ford, J., Wagner, E.C., Ochkin-Koenig, O., Franck, M., Weis, D., Meesters, G. M.H., van Ommen, J.R., 2024. Stirrer design for improving fluidization of cohesive powder: a time-resolved X-ray study. *Chem. Eng. Sci.* 294, 120069. <https://doi.org/10.1016/j.ces.2024.120069>
- Wu, K., de Martín, L., Coppens, M.-O., 2017. Pattern formation in pulsed gas-solid fluidized beds: the role of granular solid mechanics. *Chem. Eng. J.* 329, 4–14. <https://doi.org/10.1016/j.cej.2017.05.152>
- Wu, K., Galli, F., de Tommaso, J., Patience, G.S., van Ommen, J.R., 2023b. Experimental methods in chemical engineering: pressure. *Can. J. Chem. Eng.* 101 (1), 41–58. <https://doi.org/10.1002/cjce.24533>